THE ASTRONOMICAL JOURNAL, 116:360–371, 1998 July

FLIERs AND OTHER MICROSTRUCTURES IN PLANETARY NEBULAE. IV. IMAGES OF ELLIPTICAL PNs FROM THE *HUBBLE SPACE TELESCOPE*

BRUCE BALICK AND J. ALEXANDER
Department of Astronomy, University of Washington, Box 351580, Seattle, WA 98195-1580; balick@astro.washington.edu, jalex@u.washington.edu
ARSEN R. HAJIAN
US Naval Observatory, 3450 Massachusetts Avenue, NW, Washington, DC 20392-5420; hajian@fornax.usno.navy.mil
YERVANT TERZIAN
Department of Astronomy and National Astronomy and Ionosphere Center, Cornell University, Ithaca, NY 14853-6801; terzian@astrosun.tn.cornell.edu
MARIO PERINOTTO
Dipartimento di Astronomia e Scienza dello Spazio, Università di Firenze, Largo Enrico Fermi 5, I-50125 Firenze, Italy; mariop@arcetri.astro.it
AND
P. PATRIARCHI
Centro per l'Astronomia Infrarossa e lo Studio del Mezzo Interstellare, CNR, Largo Enrico Fermi 5, I-50125 Firenze, Italy; patriarchi@arcetri.astro.it
Received 1998 February 17; revised 1998 March 19

ABSTRACT

We report new results from high spatial resolution Wide Field Planetary Camera 2 imaging studies of "FLIERs" and other microstructures in the planetary nebulae NGC 3242, 6826, 7009, and 7662. Most FLIERs have head-tail morphologies, with the tails pointing outward from the nucleus. Ionization gradients that decrease with distance from the nebular center are ubiquitous. These are consistent with an ionization front in neutral knots of density $\approx 10^4$ cm^{-3}. Can neutral knots account for the properties of FLIERs? We compare two broad classes of possible explanations for FLIERs with the new images: high-speed bullets ramming through the shells of planetary nebulae, and photoevaporated gas swept by winds into head-tail shapes. Both classes of models fail basic consistency tests. Hence an entirely new conceptual paradigm is needed to account for the phenomenology of FLIERs.

Key words: planetary nebulae: general —
planetary nebulae: individual (NGC 3242, NGC 6826, NGC 7009, NGC 7662) —
stars: mass loss

1. INTRODUCTION

FLIERs ("fast low-ionization emission regions") and most other microstructures in planetary nebulae (PNs) are low-ionization knots of scale size $\approx 10^{15}$ cm that tend to come in pairs equidistant from, and on opposite sides of, the nucleus. FLIERs were first revealed in narrowband ground-based images of PNs (e.g., Balick 1987; Schwarz, Corradi, & Melnick 1992). They were first discovered in elliptical PNs (EPNs) and seem to be most common in this class of objects. The FLIERs studied in the present program are found in four particularly bright and easily studied EPNs, NGC 3242, 6826, 7009, and 7662.

Kinematic studies (e.g., Balick, Preston, & Icke 1987, hereafter BPI) have revealed that (1) velocities of FLIERs are supersonic (Mach number $\mathcal{M} \approx 5$) relative to the sound speed of the gas around them, (2) members of a pair exhibit equal but opposite velocities with respect to the nebula's systemic velocity, and (3) FLIERs have far larger Doppler shifts (and concomitantly smaller kinematic ages) than the more slowly expanding gas of the PN shells that surrounds them. The microstructures and their origins and evolution are the focal point of this paper.

Before proceeding, we shall define some morphological terms used throughout this paper. EPNs are generally described as follows (Balick 1987): A central star or "nucleus" lies at their center. Separating the nucleus from most of the nebula is an inner dark "cavity," which, in hydrodynamic models, is associated with an expanding wind-heated bubble. The cavity is always surrounded by a bright "rim" or "thin shell," outside of which lies a fairly amorphous and thick "shell" of nebulosity. The rim is believed to be former shell gas that has been snowplowed by the bubble's expansion. Kinematic studies show that rims and shells have prolate geometry.

The surface brightness of the shell is generally higher along its minor axis, as if a "thick disk" or "torus" lay in the nebula's equatorial plane. The cavity, rim, shell, and torus almost all share the same symmetry axis. The torus is believed to be created during the ejection of the outer layers of the star during its asymptotic giant branch evolution. Its relatively high thermal pressure forces the subsequent growth of the nebular rim and shell to be fastest along the nebular symmetry axis.

FLIERs are found in roughly half of the EPNs. Generally they come in pairs along the symmetry axis, and this is the case for the nebulae discussed here. There are exceptions: the FLIERs of Hubble 4 lie close to the minor axis (López, Steffen, & Meaburn 1997), and in some cases the FLIERs appear to lie along the lateral edges of a pair of cones lying on the symmetry axis, as if they were ejected by a precessing source (e.g., Fleming 1; López, Roth, & Tapia 1993; Lopez, Meaburn, & Palmer 1993; Cliffe et al. 1995). Returning to the microstructures, we begin with a summary of the concepts that have been considered to explain their physical nature.

Edge instabilities.—The locations of microstructures at the very periphery of many EPNs led Kahn & Breitschwerdt (1990) and Breitschwerdt & Kahn (1990) to suggest that some microstructures are instabilities that form in situ when the advancing ionization front (IF) breaches

the outer edge of the dense shell and accelerates. This concept accounts for some low-velocity knots near the edges of shells, but it cannot account for the large red/blueshifts or the symmetries of pairs of FLIERs.

Stellar bullets.—Balick et al. (1993, 1994, hereafter Papers I and II, respectively) and Hajian et al. (1997, hereafter Paper III) found that FLIERs consist of strongly N-enriched material (by about a factor of 5). This, their highly supersonic Doppler shifts, and their relatively short kinematic ages suggest the conclusion that FLIERs might be young supersonic bullets. (Alexander & Balick [1997] showed that the "ionization correction factor" method used to measure abundances in Papers I, II, and III overestimate the N/O ratio in FLIERs by a factor of 2. Nonetheless, some degree of local N/O enrichment appears incontestable.)

Nebular bullets.—Are FLIERs bullets somehow formed in or near the shell by interacting stellar winds? The hydrodynamic models of interacting winds have proved successful at explaining the large-scale structure of PNs (Kwok, Purton, & FitzGerald 1978; Kahn & West 1985; Balick 1987; Mellema 1995; Mellema & Frank 1995). However, these models fail to account for the formation of dense, low-ionization, high-speed knots near the nebular symmetry axis. The overwhelming problem is that fast stellar winds (≥ 150 km s^{-1}) that converge through the nearby prolate inner (reverse) shock have vastly subcritical cooling rates for condensation into small, stable knots (Icke, Balick, & Frank 1992).

Slower winds (< 150 km s^{-1}) in the proto-PN stage of EPNs might produce streams of rapidly cooling gas that slide along the prolate contact discontinuity and splash as they converge at the polar axis (Frank, Balick, & Livio 1996), much like the formation of Herbig-Haro objects in young stellar outflows. However, Dwarkadas & Balick (1998) found that shear-induced instabilities along the cavity walls effectively disrupt those converging flows. Hence, knots with the properties of FLIERs are, at best, too transitory an evolutionary stage to constitute a robust explanation for the very frequent appearance of FLIERs in EPNs.

Problems arise for all bullet models. Bullets would be expected to appear as bow shocks with tails opening inward toward the star and heads that are most highly ionized at their leading edges. In contradiction, tails, when they are seen (e.g., the cometary nebulae of NGC 7293), open outward. Ground-based long-slit spectroscopic data obtained with 1″.5 seeing strongly suggested that all FLIERs have rapidly decreasing ionization with radius from the nucleus. These ionization gradients argue that microstructures are associated with the IFs of neutral knots.

Wind-accelerated photoevaporation flows from neutral knots.—Perhaps FLIERs are associated with gas that has been accelerated by immersion in some invisible higher speed wind. Suppose that neutral knots are directly exposed to dilute stellar winds. It is easy to show that the transfer of momentum from the stellar wind can accelerate $\leq 10^{-4}\,M_{\odot}$ of photoevaporated gas to speeds ≥ 30 km s^{-1} during the kinematic lifetimes of FLIERs.

But this conceptual idea is flawed. The primary problem is that the knots will appear as bullets—a concept already found dubious (see above). In addition, the wind cannot reach the knots, at least not at their present locations. That is, the momentum flux of any stellar wind effectively ends at the shock on the leading edge of the rim, far from the present locations of the FLIERs. Even if the winds somehow managed to reach the knots when they were situated at the edge of the bubble, standoff shocks and a thick layer of hot (shock-heated) gas would insulate the photoablated gas from direct contact with the winds (Dyson, Hartquist, & Biro 1993; Lizano et al. 1996; Henney et al. 1996). In short, although it has not been ruled out through direct observations, the concept of wind acceleration seems unlikely.

Oort-Spitzer rockets.—In this model (Oort & Spitzer 1955; Mellema et al. 1998), no winds are needed to account for the high velocities of the knots. Instead, neutral knots are accelerated radially in reaction to "exhaust" gas formed by photoevaporation. A knot will attain a supersonic speed near the end of its life, when almost all of its original mass has been lost. This reveals the problem with the concept: knots with substantial radial velocities are extremely ephemeral. What is more, a collection of neutral knots with random masses or ages should show a variety of Doppler shifts at any given time, whereas FLIERs are very well characterized by a single red- or blueshift (BPI). A kinematic study of numerous neutral knots that are exposed to ionizing radiation in the Helix Nebula (Meaburn et al. 1998) showed that none of them have the velocities expected of rockets.

A new paradigm is needed for understanding FLIERs. The next logical step is to observe the morphologies of FLIERs on size scales like that of the IFs (i.e., the mean free path of ionizing photons, $\leq 0''.1$ at 1 kpc). This allows their ionization structure to be probed in detail. Also, any bow shocks or photoevaporation flows from knots might become visible in high-resolution images. Such images might provide decisive pieces of the observational puzzle. For these reasons we obtained images of FLIERs and their host PNs in a variety of emission lines using the Wide Field Planetary Camera 2 (WFPC2) on the *Hubble Space Telescope* (*HST*). The observational results are presented and discussed in this paper.

2. OBSERVATIONS

The four targets of this study, NGC 3242, 6826, 7009, and 7662, were observed using the WFPC2 (Holtzman et al. 1995) for two orbits each on 1996 April 19, January 27, April 28, and January 5, respectively. No problems were reported during the observations. A variety of filters and exposure times were used to obtain both deep images (total integrations up to 1200 s in repeated exposures) and unsaturated images (single 100 s exposure) in different emission lines.

Aside from NGC 7009, the targets were observed within the PC camera ($0''.045$ pixel^{-1}). Since the wine-bottle–shaped PN NGC 7009 overfills the field of view of the PC, its center was offset and the nebula was oriented diagonally to maximize its PC visibility. The rest of the nebula fell into various WF cameras ($0''.10$ pixel^{-1}). The images presented here have been "drizzled" onto a uniform grid of pixels, each $0''.10$ size, using software supplied by STScI. Because the structures of NGC 7009 are all well resolved in the PC portion of the images, very few nebular details were suppressed by regridding the data to larger pixels.

A pixel of size $0''.10$ corresponds to 100 AU (0.0005 pc) at a distance of 1 kpc, a distance that is typical for all of the targets. However, the actual distances are only poorly

known, as a glance at Table 1 makes obvious. In view of these huge disagreements, we must be cautious about using physical sizes in subsequent discussions.

The distances shown in Table 1 are averages of the best values available in the catalog of Acker et al. (1992). Please note that the errors quoted for individual distances are often smaller than the dispersion of the values in the catalog, meaning that systematic errors in each of the tabulated values are large. Values of $T_{\rm eff}$ were adopted from studies of Zanstra temperatures. To avoid problems arising from the highly uncertain distances, we derived luminosities L from $T_{\rm eff}$ and the most recent evolutionary-track calculations for a star of mass $M = 0.605\ M_{\odot}$ by Blöcker (1995). (The spectrum of the star was assumed to be a blackbody.) The terminal velocity v_{∞} and mass-loss rates $\dot{M}$ are derived by rescaling the best available measurements in the literature for the adopted value of the stellar radius (not shown), which was derived from L and $T_{\rm eff}$.

Hereafter we shall use the following abbreviations: Hα = H I λ6563, He II = He II λ4686, [N II] = [N II] λ6583, [O I] = [O I] λ6300, [O II] = [O II] $\lambda\lambda$(3726 + 3729), [O III] = [O III] λ5007, and [S II] = [S II] $\lambda\lambda$(6717 + 6731). "Low- (high-) ionization" regions are characterized by the dominance of N^+ and O^+ (N^{++} and O^{++}) within the PN's H II region. All velocities are referred to the systemic nebular velocity (average Hα velocity).

The filters, their bandwidths, and the dominant emission lines in their passbands used for the present images are F375N, 26 Å, [O II]; F487N, 22 Å, He II; F502N, 27 Å, [O III]; F631N, 31 Å, [O I]; F656N, 22 Å, Hα; F658N; 28 Å, [N II]; and F673N, 47 Å, [S II]. The images were placed on a photometrically calibrated intensity scale using the SYNPHOT package in the IRAF/STSDAS software. The system throughput in the F375N filter is poor. Thus no [O II] images were usable.

Cosmic rays (CRs) were removed from repeated exposures using standard software in STSDAS. In a few cases only single exposures were made. In this case IDL routines written locally by E. Deutsch of the University of Washington were run using very conservative settings to detect CRs by their sharp edges. An inspection of the residuals made by subtracting the CR-corrected images from the corresponding raw image shows that no small nebular features were affected, and that only minor CRs with low amplitude remain after the CR removal routines have been run. We have no reason to suspect that improperly removed CRs influence any of the scientific conclusions reached in this paper. The passbands of F656N and F658N "leak" small but well-known amounts of [N II] and Hα, respectively. The leakage was calibrated using IRAF/SYNPHOT. Appropriately scaled images through one filter were subtracted from the other to correct for this problem. The H^+ recombination continuum was removed by appropriately scaling and subtracting the Hα image. No correction for the He^{++} recombination continuum was attempted, since the F469N images are noisy and because no FLIERs are found in the zone in which He^{++} is abundant.

The accuracy of the final photometric calibration was checked by comparing the total nebular emission-line fluxes of NGC 7662 through many of the filters with integrated continuum-free ground-based fluxes measured by Lame & Pogge (1996). The results agree to 5%. Filter throughput calibrations by STScI staff (B. Whitmore 1997, private communication) give equally consistent results.

Finally, the alignments of images through various filters were checked by measuring the centroid position of the nucleus and/or field stars. The misalignments are typically 0.4 pixels, and always less than 0.6 pixels, prior to any correction. The offsets were measured for all targets and found to be consistent to within 0.3 pixels. Luckily, the filters with the largest average alignment differences are those of high-ionization lines that show the most amorphous nebular structure. Fortuitously, FLIERs are best seen in [O I], [S II], and [N II] images, all of which are aligned to about 0.1 pixels in the uncorrected images. Furthermore, we conducted numerical experiments in which we shifted a test image with fine-scale structure by various fractions of a pixel and then shifted it back to its original position. After subtracting the twice-shifted image from the original, we found that any attempt to align the images by more than 0.2 pixels was likely to cause more harm than good. Hence no image alignment has been applied to any of the images.

3. RESULTS

For display purposes, the image intensities were normalized to their own peaks and converted to logarithms. The most distinct ionization zones—He^{++}, O^{++} and N^+—are shown in Figure 1 as blue, green, and red, respectively. The FLIERs and most other microstructures are conspicuous as sharply articulated red features near the nebular edges. They appear to lie well outside the walls of an apparently prolate bubble that surrounds the nucleus. Note the

TABLE 1

OBSERVED PROPERTIES OF THE NUCLEI OF THE TARGET NEBULAE

Planetary Nebula	Spectral Type	$T_{\rm eff}$ (10^3 K)	log $(L/L_{\odot})$[a]	Average Measured Distance[a] (kpc)	Expansion Distance[b] (kpc)	Expansion Age[b] (yr)	v_{∞} (km s^{-1})	$\dot{M}$ ($M_{\odot}$ yr^{-1})
NGC 3242.....	sdO (1)	60 (4)	3.48	0.9	0.47	1900	2200 (8)	8×10^{-10} (8)[c]
NGC 6826.....	O3f(H) (2)	45 (5)	3.79	1.0	...	...	1750 (5)	5×10^{-8} (9)
NGC 7009.....	O(H) (2)	88 (6)	3.75	1.0	0.60	1900	2770 (6)	2×10^{-9} (10)
NGC 7662.....	Continuous (3)	120 (7)	3.67	1.2	0.96	1300	...	...

[a] Average of distances complied by Acker et al. 1992.

[b] Terzian 1998.

[c] We adopted the logarithmic mean of the range of values quoted, 8×10^{-9} and 8×10^{-11}. The entry is very uncertain.

REFERENCES.—(1) Heap 1986; (2) Méndez 1991; (3) Aller 1976; (4) Acker et al. 1992; (5) Perinotto, Cerruti-Sola, & Lamers 1989; (6) Cerruti-Sola & Perinotto 1989; (7) Harrington et al. 1982; (8) Hamann et al. 1984; (9) from (5), modified for stellar radius adopted herein; (10) from (6), modified for stellar radius adopted herein.

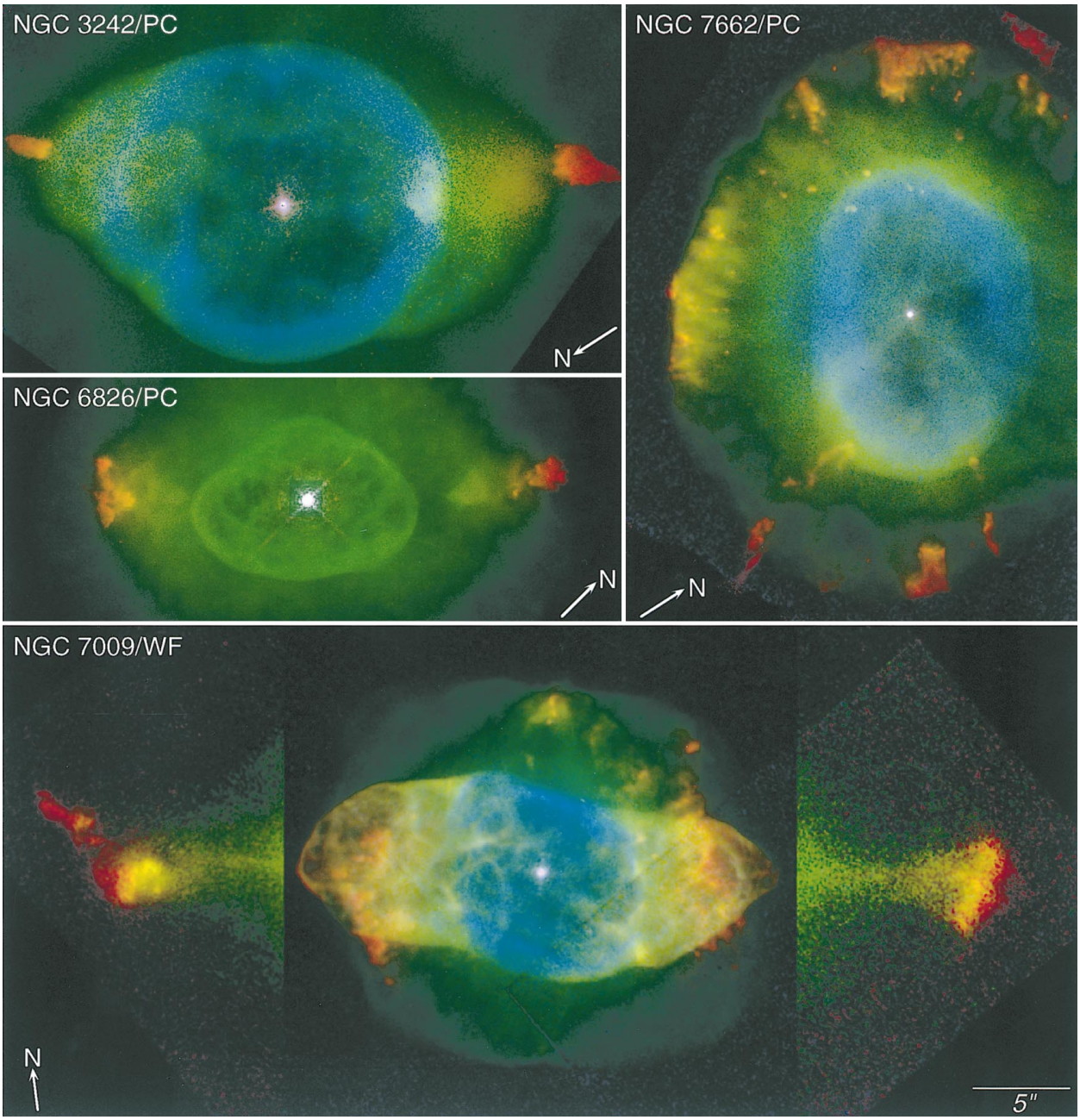

FIG. 1.—WFPC2 images of PNs containing FLIERs. Pixels are 0.″10 for NGC 7009 and 0.″045 for the other nebulae. The [N II] image is shown in red, the [O III] in green, and the He II λ4686 in blue. The north direction is approximate.

relationship of the low-ionization FLIERs and other microstructures to the more highly ionized nebular background: almost no trace of O^{++} is seen in the FLIERs except for NGC 7662.

The ionization structure of the FLIERs is presented in Figure 2. In this case blue, green, and red correspond to Hα, [N II], and [O I]. [S II] emission (not shown) is similar to [O I], except that it often becomes weak in some regions of brightest [N II] and [O I]. Presumably, this is because the [S II] line is effectively collisionally quenched at densities n above about 10^4 cm^{-3} whereas the other forbidden lines are quenched only at densities $n > 10^5$ cm^{-3}. If so, this provides a crude estimate of the density and, hence, the mean free path of the hard ultraviolet photons that reach the IF. If photons that reach the IF are characterized by 50 eV, then their mean free path (i.e., the approximate thickness of the IF) is $3n^{-1}$ pc, or 1.4 PC pixels, for a distance of 1 kpc and a density of 10^4 cm^{-3}. This is very close to the observed separations of the [N II] and [O I] filaments along the star-facing edges of all of the microstructures.

Individual microstructures are characterized by many similarities and some differences. The similarities are primarily their thin widths (as defined in Fig. 2) and flaring shapes, with their apexes generally pointed toward the central star and tails generally pointed radially outward. This is obviously the case for all of the FLIERs in NGC 3242 and NGC 6826 and most of the microstructures of NGC 7662. As we shall see, these are new and very significant morphological results. The morphology is reminiscent of the cometary nebulae observed in NGC 7293 by O'Dell & Handron (1996).

One-dimensional "profiles" of emission-line surface

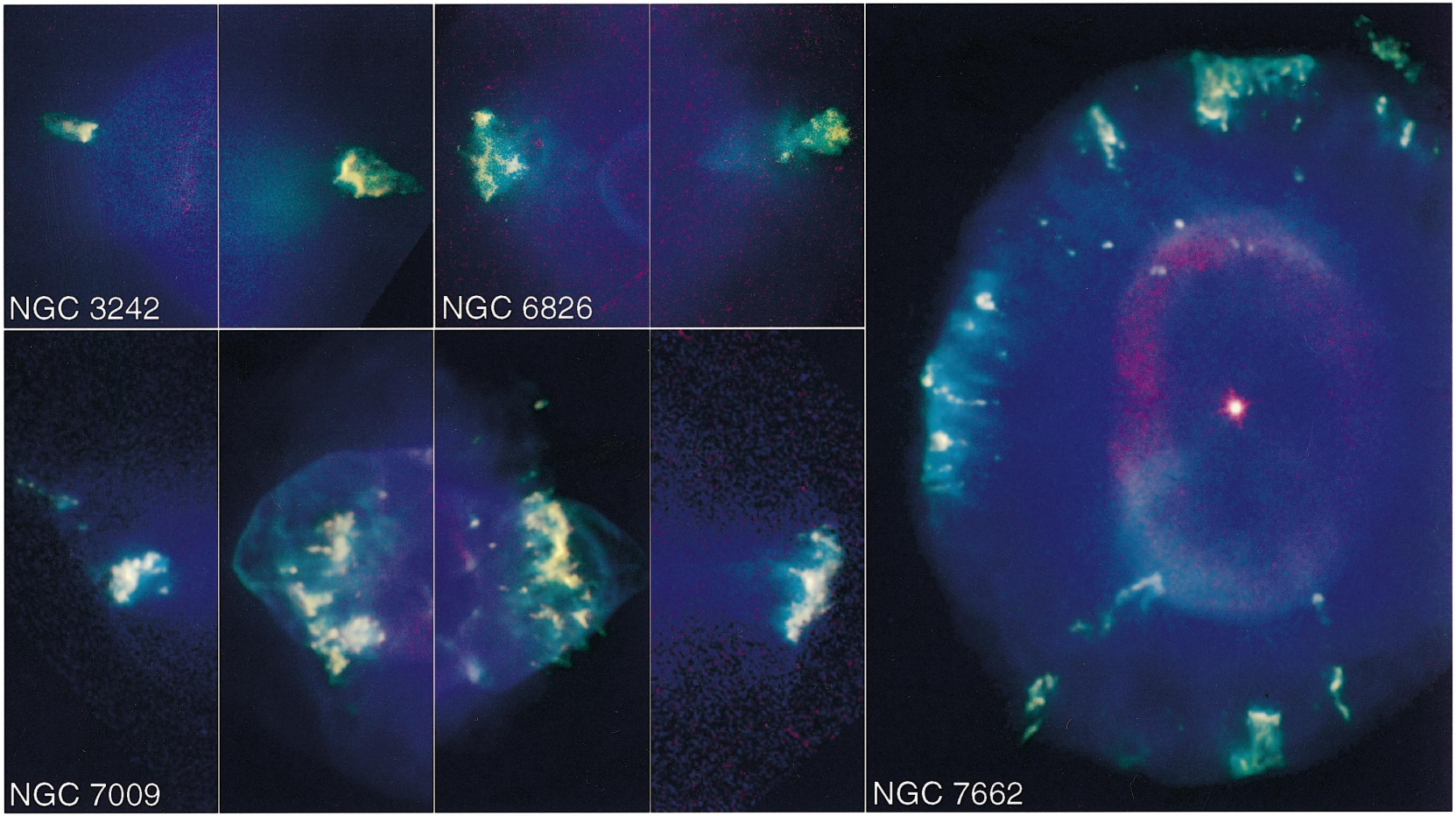

FIG. 2.—Similar to Fig. 1, except that FLIERs and other microstructures are highlighted. The [O I] image is shown in red, the [N II] in green, and the Hα in blue. Gradients in the colors imply that the respective emission regions are offset from one another.

brightness are displayed in Figure 3 for many of the microstructures. These profiles were made by rotating the images until a pair of FLIERs was aligned horizontally and then drawing a rectangular box 10 pixels high that encompassed both of the brightest filaments. The brightnesses were then averaged over the 10 pixel height to produce a one-dimensional brightness distribution, or "profile."

Next we describe the most salient features of microstructures in the individual targets, starting with the simplest examples.

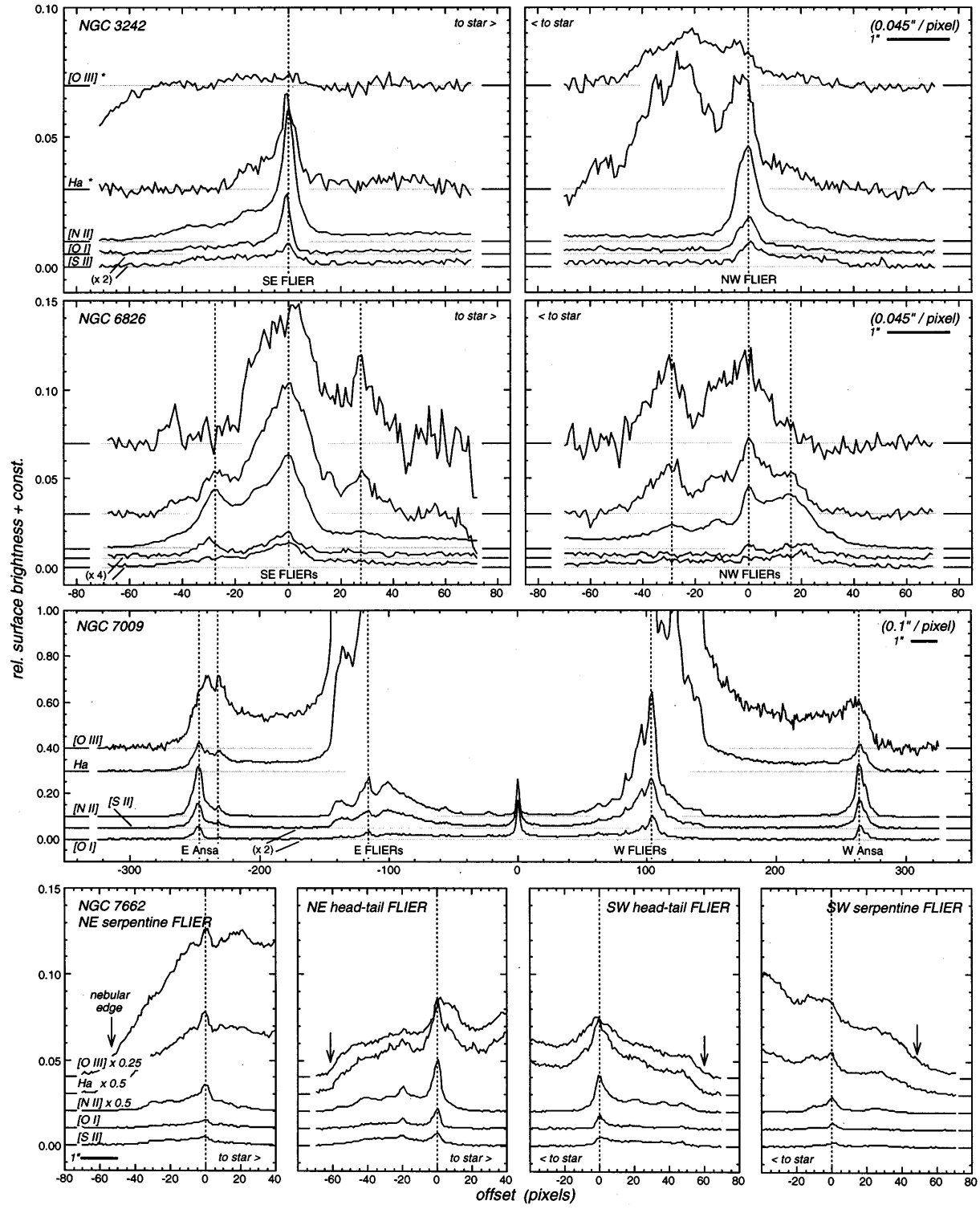

FIG. 3.—Emission-line brightness distributions ("profiles") made along axes passing through the FLIERs and ansae of the program targets. For each nebula, the lines plotted are noted along the left edge of the left panels. The vertical units are surface brightnesses, the scales of which are the same for all lines unless indicated otherwise. A constant offset has been added for clarity (brightness zero points are indicated along the sides of each panel and under each profile). The pixel size is 0".1 for NGC 7009 and 0".045 for the other nebulae. Baselines have been fitted and removed in those profiles marked with an asterisk. A dotted vertical line passes through the peak of the [N II] brightness and is shown as a fiducial. Ten data lines are averaged together in forming each pixel shown here, except for NGC 7662, for which 15 lines of data were averaged. For NGC 7662, the data were extracted from an artificial slit passing through the serpentine FLIERs at 4 and 10 o'clock with respect to the nucleus in Fig. 1. A similar slit at 5 and 11 o'clock was used for the head-tail FLIERs.

NGC 3242.—The images of the FLIERs are found in the top left panels of Figures 1 and 2. Two well-resolved FLIERs are found at the ends of loops emanating from the edges of the central bubble surrounding the star. Each FLIER consists of a head (relatively bright filament) with a fainter radial tail. NGC 3242 is alone among all our targets in exhibiting this geometry of single FLIERs connected by loops (or any converging structures) to the region near the star.

Little if any [O III] line emission is associated with the southeast FLIER. Both FLIERs exhibit Hα emission with about the same surface brightness and size scale as [N II]. The extended [O III] and Hα emission between the nucleus and the northwest FLIER is associated with the loop of emission seen on the left side of the image of NGC 3242 in Figure 1.

As discussed at the beginning of this section and seen clearly in Figure 3, there is strong evidence that the [S II] lines are being quenched by collisions in the brightest regions of the FLIERs. Hence the densities in the filaments exceed 10^4 cm^{-3}. This clears up a puzzle in earlier ground-based spectroscopic studies (Paper I) of the [S II] λ6717/λ6731 line ratio, in which the densities in the FLIERs and that in the nearby gas appeared to be almost the same. The present subarcsecond images show that the true densities are higher than 10^4 cm^{-3}.

Ionization gradients are discernible across the bright filaments in the heads of the FLIERs (Fig. 2). The ionization gradient argues that the filaments are IFs. It is possible that a shock provides some additional heating to the IF; nonetheless, the shock will not have any observable effect on the emerging spectrum except under extreme conditions (Dopita 1997).

Ground-based kinematic studies of the FLIERs by BPI show that the FLIERs have Doppler shifts of ±25 km s^{-1} relative to the systemic velocity of the nebula (the true velocities are probably higher because of projection effects). The Doppler shifts of the loops that connect the FLIERs to the bright rim surrounding the star start at the nebular systemic velocity at the rim and increase linearly to the Doppler shifts of the FLIERs at their endpoints.

NGC 6826.—The FLIERs appear to be an aggregate of individual low-ionization, comet-like microstructures, each of which resembles the FLIERs in NGC 3242. Like the FLIERs of NGC 3242, knots in the FLIERs of NGC 6826 exhibit ionization gradients (Fig. 2). Also like NGC 3242, ground-based observations (BPI) show that the gas accelerates between the nearby tips of the prolate rim and FLIERs, culminating at the red/blueshifts of the FLIERs of ±25 km s^{-1}.

The [S II] and [O I] lines are very weak in the present images of the northwest FLIER complex (Fig. 3). Even so, the profiles in Figure 3 again argue that the [S II] λλ6717, 6731 lines are quenched in the brightest regions relative to Hα, [N II], and [O I] emission, suggesting that earlier assertions that knots have the same density as their surroundings (Paper II) are erroneous.

Aside from its aggregates of knots, the FLIERs of NGC 6826 are distinguished from those in NGC 3242 in another interesting way. Instead of loops, a "vee" of high-ionization material seems to connect the northwest FLIER (and perhaps the southeast one also) to the nearest tip of the bright prolate rim surrounding the nucleus. This vee, which opens with radius, seems to have many of the same symmetries as do the aggregates of FLIERs a bit farther downstream. Interestingly, neither the edges nor the vertex of the vee is brightened, so the observed emission does not arise from a thin conical surface layer.

NGC 7009.—The global structure and ionization have been described by Bohigas, López, & Aguilar (1994) and Paper II. There are two pairs of low-ionization regions in NGC 7009. The inner pair (called "caps" in Paper II) is found near the tips of the core of the nebula. Their red/blueshifts are about ±40 km s^{-1} (BPI). The complex set of inner microstructures are authentic FLIERs. The outer pair, which appear connected to the core by thin jets or streams, have been called "ansae," or handles (Aller 1941). Their measured Doppler shifts are only about ±5 km s^{-1}, perhaps the result of projection effects; however, Reay & Atherton (1985) argue that after correction for projection effects the true velocities of the ansae are 160(D/2) km s^{-1}, where D is the distance in kiloparsecs. Both pairs of FLIERs show the usual decreasing gradient of ionization with distance from the star, particularly in the PC image.

Consider the ansae. Are they FLIERs despite their small Doppler shifts? An inspection of Figures 1 and 2 leaves a strong impression of a spout or jet of gas that connects the ansae to the tips of the prolate bubble. The jets are relatively faint, very thin and straight filaments in [N II] around which is a smooth sheath of higher ionization (Hα and [O III]) gas. The sheath opens slightly with increasing radius from the tips of the bubble. No symptoms of instabilities or shear flows appear. Therefore, the collimation of the jets appears to be imposed at the extreme tips of the prolate bubble.

The jets end at the ansae, whose state of ionization is considerably lower. If such jets interact supersonically with a smooth, ambient medium, then bow shock should result. A deep image of the ansae (Fig. 4) shows that the ansae lie at the outer extrema of features that appear to be bow shocks. However, the effective shock speed, and hence heating of the shocked gas, is expected to be largest in the head of the shock. The relatively low ionization and modest temperatures at the heads of the bow shocks containing the ansae are precisely the reverse of theoretical expectations.

The long-slit observations of Paper II showed that the

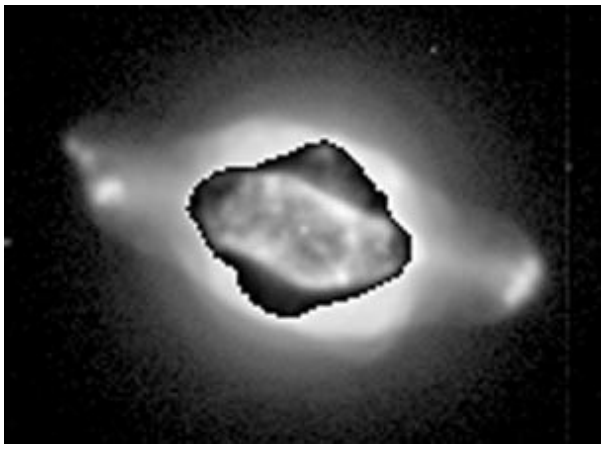

FIG. 4.—A 60 s exposure in subarcsecond seeing of NGC 7009 taken through an Hα + [N II] filter using the prime-focus CCD of the 4 m Mayall Telescope at Kitt Peak National Observatory (adapted from Balick et al. 1992). North is up and east is to the left. The inset shows the bright inner regions obtained from a 10 s exposure by G. Jacoby using the same instrumentation.

densities measured from the [S II] lines are about 1000 cm^{-3} with only a slight increase where the slit intersects the ansae. Since there is no sign of collisional quenching in the [S II] line profile (Fig. 3), the compression of the emitting gas appears to be small. Consequently, it is not clear why the emission measures are so enhanced in the ansae.

The temperatures of the ansae and the jet were found to be 10^4 K with only small variations though the ansae (Paper II). This is expected for an ionization front. A deep image of the ansae (Fig. 4) shows that the ansae lie at the outer extrema of bow shocks in which the ionization state is lowest at the heads. This is the exact reverse of expectations, in which the highest shock velocities, temperatures, and ionization states are reached in the heads of bow shocks.

In summary, the ansae seem to be low-ionization material being pushed by the jets across the plane of the sky. The jets appear to be photoionized. The low ionization of the ansae is puzzling. The lack of a substantial density enhancement in the ansae argues that no IF is trapped in the ansae. It will be interesting to see if future high-dispersion observations show that the line widths of Hα and [O III] lines flare at the interface, as is sometimes seen in Herbig-Haro objects (e.g., Böhm & Goodson 1997).

Let us return briefly to discuss the inner pair of FLIERs. Both are complex networks of smaller FLIERs projected onto the bright, highly structured interior of the nebula. The individual morphologies of the microstructures appear to be complicated though generally reminiscent of the FLIERs seen in NGC 3242 and NGC 6826 (but not the ansae above). The networks of filamentary FLIERs lie roughly normal to the nebular symmetry axis, as if they were formed where a stellar wind rams into a filament, sheet, or the inner edge of a disklike region and shreds it (i.e., forming Vishniac thin-shell or Rayleigh-Taylor instabilities). Judging from their substantial Doppler shifts, the inner FLIERs lie along an axis that is inclined to the plane of the sky and the inner regions of the nebula. This seems to be a peculiar result, unless the orientation of the symmetry axis of the nebula precesses between successive FLIER formation events (see, e.g., Cliffe et al. 1995).

NGC 7662.—This is the most complex of the nebulae studied here. Morphologically, a thin but well-resolved elliptical rim separates a dark cavity around the star from a fairly smooth shell or halo of more amorphous gas at larger radii. As in other nebulae, this rim is almost certainly gas swept up by the growing bubble where the gas is compressed between a weak shock and a contact discontinuity.

A dozen microstructures can be seen around the nebular periphery of NGC 7662. A great range of morphologies is apparent, from tiny, tailless knots to almost radial serpentine features. They are most prominent in lines of very low ionization even though the gas that surrounds them is much more highly ionized. There are some exceptions, all near the 9 o'clock direction in Figures 1 and 2, in which bright Hα and [O III] counterparts of the low-ionization microstructures are apparent.

Long-slit spectroscopic observations of selected microstructures were made in Paper I. The densities were found to be on the order of 10^3 cm^{-3} throughout the microstructures and nearby portions of the nebular shell. However, Figure 3 suggests that the [S II] lines are partially quenched in the brightest regions of the filaments. As in all of the other target PNs, temperatures measured from [N II] lines show no variations near the microstructures.

The microstructures of NGC 7662 fall into four morphological classes, "head-tail," "serpentine," "tail-head," and "specks." Head-tail filaments are cometary features much like those in NGC 3242 and NGC 6826. The brightest of these are found near 12 and 6 o'clock in Figure 1. Serpentine features extend radially from the rim to the edge of the nebula and beyond. These come in two pairs: one at 5 and 11 o'clock, and the other at 1 and 7 o'clock in Figure 1. Tail-head microstructures lie exclusively in a zone near 9 o'clock, where a complex of stubby radial features at the perimeter of the shell is evident. They are also distinguished by bright Hα and [O III] counterparts, as noted earlier. Specks are nearly unresolved knots lying irregularly between the rim of the hot bubble and some of the serpentine microstructures in the upper part of the images in Figures 1 and 2. We do not consider them further.

Next we digress briefly to review the kinematics of the microstructures of NGC 7662 and place these in the context of the interesting large-scale nebular kinematics. Refer to the Hα and [N II] kinematic images of NGC 7662 (Fig. 5), in which relative red/blueshifts of the microstructures and the nebula (measured from the long-slit echelle observations of BPI) are coded in colors. Red represents redshifts, blue indicates blueshifts, and green implies gas close to the systemic velocity of the nebula. The ground-based echelle observations on which Figure 5 is based were measured on a $1'' \times 2''$ grid of points in $1''.5$ seeing. The data were interpolated to a $1'' \times 1''$ grid when making the figure.

The Doppler shifts of the microstructures are best seen in the [N II] kinematic image. The serpentine microstructures have the largest red/blueshifts (± 30 km s^{-1}; BPI) and are true FLIERs. As in other nebulae, the velocities are antisymmetric with respect to the nucleus. The head-tail microstructures have modest Doppler shifts; however, the correction for projection effects is likely to be considerable. For this reason we shall classify the head-tail microstructures as FLIERs. The tail-head microstructures on the east edge of the shell have small Doppler shifts. Their status as true FLIERs is debatable.

The global kinematics is best seen in the Hα kinematic image. The relatively subtle colorations are the result of the large thermal broadening of the Hα line, which "muddies" red colors to yellow and blue colors to cyan. A seemingly complex pattern of Doppler shifts emerges. Red/blueshift gradients are seen along the nebula's major and minor axes.

A relatively simple and plausible heuristic way to interpret the pattern is shown schematically in Figure 5. Suppose that the true nebular structure is that of a mostly filled prolate shell with a central cavity, whose major axis lies near P.A. $\approx 45°$ and has an inclination angle of 20°–30°. The expansion of this tilted prolate ellipsoid and the bright rim on its inner surface accounts for the Doppler-shift gradient along the nebula's major axis. A torus lies within the prolate shell and shares its symmetry axis (only its midplane is shown in Fig. 5). The gradient in Doppler shift along the shell's minor axis is identified with the expansion of this tilted torus. The head-tail and serpentine FLIERs lie fairly close to the symmetry axis of the prolate shell, and the tail-head microstructures outline the east edge of the torus. Note that a similar spatio-kinematic pattern is also seen in NGC 6543 (e.g., Miranda & Solf 1992).

We now return to the discussion of the various types of FLIERs.

Serpentine FLIERs are the fastest-moving microstruc-

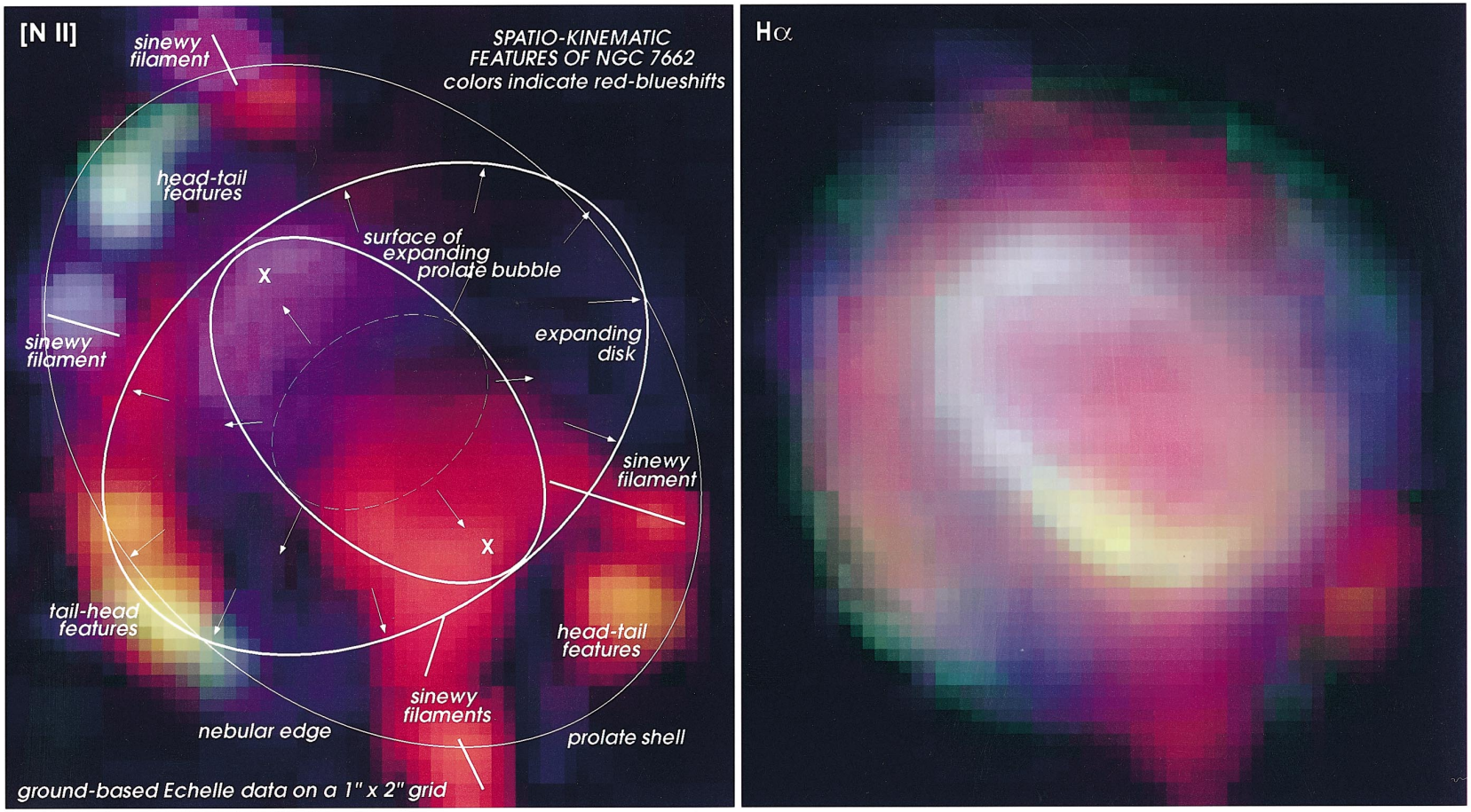

FIG. 5.—Spatio-kinematic features of NGC 7662. These images have been reconstructed from a series of long-slit echelle observations by Balick, Preston, & Icke (1987) on a 1″ × 2″ grid of points. Colors represent red- or blueshifts relative to the systemic velocity of the nebula. [N II] and Hα observations are shown in the left and right panels, respectively. The overlay shows various features discussed in the text. Surrounding the star is a prolate elliptical cavity formed by an expanding, wind-heated bubble. Crosses mark the projection of the tips of the prolate bubble onto the sky. The bubble is surrounded by a bright rim of gas on the inside edge of an expanding prolate ellipsoidal shell. An expanding torus or disk lies along the minor axis. The bubble, rim, shell, and torus all share the same symmetry axis in P.A. $\approx 45°$, which is tilted by about 30° from the plane of the sky. Head-tail FLIERs are found on the outer edge of the prolate shell and near its symmetry axis. Serpentine FLIERs are found in the same region but farther from the axis. Tail-head microstructures appear near the east edge of the expanding torus.

tures. They seem to cut through the far more highly ionized gas of the prolate ellipsoidal shell. Unless they are highly transient, the low ionizations of serpentine FLIERs are difficult to understand. Although their kinematic structure is not well sampled, a glance at Figure 8 in BPI shows that the Doppler shifts of the serpentine features increase with distance from the nucleus. This suggests that the emitting gas is accelerating with radius. Curves and kinks along the serpentine features could be the results of shear instabilities. As shown in Figure 3, the bright heads of the serpentine FLIERs are visible in all emission lines.

The head-tail FLIERs lie along the nebular major axis near the boundary of the shell, at 6 and 12 o'clock in Figures 1 and 2. Their tails end abruptly at the edge of the shell, which argues that these FLIERs lie near the plane of the sky (and their true space velocities are much higher than their Doppler shifts suggest). It is significant that the tails do not extend beyond the shell. Three possible explanations are (1) the tails are the limb-brightened sides of ionization shadows in the shell behind neutral knots that are illuminated by soft recombination photons near 13.6 eV, (2) shear flows that require the dense gas of the shell in order to heat and excite them, and (3) the tails have detectable emission measures only where they are confined by the thermal pressure of the shell. Echelle observations may help to distinguish among these possibilities; however, such observations will mandate the spatial resolution of *HST*.

Tail-head microstructures are found only along one edge of the nebula's equatorial axis and may be associated with the expanding torus or disk (see Fig. 5). Their thin tails point toward the star (more or less) rather than outward. They have the most prominent [O III] and Hα counterparts and among the smallest red- and blueshifts of all of the microstructures described in this paper. Nothing similar to them has been encountered in the other objects in this study. For these reasons, the tail-head structures probably have a different physical origin from other microstructures. Features much like the tail-head microstructures are seen along the entire edge of the equatorial disk of NGC 6543 (Harrington & Borkowski 1994). In both cases, the edge-instability model of Breitschwerdt & Kahn (1990) may apply.

4. THE BRIGHT RIMS

Bright rims that outline the central cavity surrounding the stellar nucleus are a common feature of round and elliptical PNs. The standard picture for the rims is that they are gas being snowplowed as the bubble expands into the undisturbed shell of material that confines it. If the growth of the bubble is supersonic, then a rim of highly compressed shell material precedes and surrounds the expanding bubble. It fills the volume between the contact discontinuity and the outer shock. The compressed gas can cool very efficiently, so it collapses into a very thin, sheetlike surface feature (and may become susceptible to various thin-shell instabilities). In any event, the rim is bounded by a shock along its leading edge, and the leading edge should (and always does) appear very sharp in projection (Fig. 1).

Images from *HST*, including those presented here, show that many bright rims have the expected sheetlike attributes of a bubble-driven snowplow, including those in NGC 6543 (Harrington & Borkowski 1994), NGC 6826 and 7009 (this study), and NGC 3195, 3918, 5882, 6578, and 6884 and IC 3568 (H. Bond 1997, private communication). A mildly surprising result from WFPC2 images is that some rims are, in fact, rather thick and easily resolved. These include NGC 2022 and 6369 (H. Bond 1997, private communication) and NGC 3242 and 7662 (this study). (Even in these cases the resolved rims have a sharp leading edge.)

A thick rim with a sharp edge might form in one of two ways: (1) magnetic fields trapped in the rim inhibit the compression of the rim or (2) the pressure of the extremely hot gas in the central bubble subsides below that of the compressed gas around it, so that the compressed gas starts to backfill the cavity. In the latter case, the forward momentum of the compressed gas maintains a shock at the sharp leading edge.

Magnetic fields should account for the prolate geometry of the rim (Chevalier & Luo 1994). However, these fields are likely to become toroidal. Thus the rim should be thicker in the equatorial plane that at the poles. This is not observed.

A drop in bubble pressure is an eventual probability for all EPNs. As long as the bubble is heated by the wind's kinetic energy ($\dot{M}v_{\rm wind}^2/2$), its thermal pressure pushes the bubble outward into the shell like a piston, creating the sharp rims. However, sooner or later the bubble will deflate, either because the bubble develops a "leak" (i.e., the shell of confining gas is punctured) or the wind's kinetic energy diminishes as the star ages (so that the cooling rate of the expanding bubble exceeds the heating rate by the stellar wind), so thickening of the rims is all but inevitable.

In NGC 3242, 6826, and 7662, there is no direct evidence of a puncture, i.e., the rim appears continuous and lies deeply embedded within the shell. On the other hand, the thermal pressure of the bubble will decline when the wind luminosity drops as the star ages (see, e.g., Pauldrach et al. 1988). Interestingly, an examination of Table 1 shows that the nucleus of NGC 3242 has the lowest value of $\dot{M}$ and $\dot{M}v_{\rm wind}^2$. The case of NGC 7662 is less obvious since the star's spectrum is featureless. Such spectra are consistent with very low values of $\dot{M}$ at the present time.

Finally, it is extremely interesting that the rims of the bubbles of a dozen EPNs (including the present four targets) show evidence of a tight network of filaments along their surfaces in various WFPC2 images. One might expect that the relatively bright filaments are regions of high density, and that between them bulges are developing as the high pressure inside the trapped hot bubble pushes outward and buckles the rim. Consequently, one might expect to see evidence of the bulges along the perimeter of the bubble where the rim projects onto the line of sight.

Quite to the contrary, an inspection of the perimeters of these bubbles (as seen in WFPC2 images) shows that all but one of them (NGC 6578) are smooth and show no trace of small bulges. It is easy to overinterpret this (e.g., the absence of bulges is the result of the tension of swept-up magnetic fields). Even so, any blobs induced by shear flows (i.e., Kelvin-Helmholtz instabilities) formed as winds may have slid along the walls of the bubble during the proto-EPN stage of the nebula's evolution (Frank et al. 1996; Dwarkadas & Balick 1998) are not in evidence.

5. CONCLUSIONS

Simply put, the very existence of low-ionization microstructures in PNs remains surprising and unexplained. Their small sound-crossing times ($\sim$100 yr) and sharp edges require that either microstructures are very young

(and have not had a chance to expand) or they are pressure confined within shocks. No means of forming such small objects in situ has ever been demonstrated (Icke et al. 1992; Dwarkadas & Balick 1998).

Hopes that the subarcsecond ($\sim 0\farcs05$) images presented here would help to clarify some of these questions have not been fully realized. We considered whether FLIERs might be bullets formed in or confined by the shell through which they move. Outflowing supersonic bullets will appear as bow shocks with tails opening toward the star. Although tails are common in most microstructures in the present survey, they almost always open in the opposite direction. Note that we reject the concept of infalling knots prima facie.

Suppose that neutral knots were immersed in some sort of nebular outflow and irradiated by the hot central star. Photoevaporated gas from the heads of the knots could then be swept into long cometary tails pointing outward, much like those seen in the Helix Nebula (O'Dell & Handron 1996). However, many problems arise with this concept. On the one hand, the gas motions in the Helix Nebula are all subsonic (Meaburn et al. 1998); on the other, in the case of the FLIERs the outflow must be highly supersonic to account for the large Doppler shifts of FLIERs. Therefore, shocked, wide bow shocks should form between the outflowing wind and the knots (Dyson et al. 1993; Lizano et al. 1996; Henney et al. 1996). The shocks will deflect the momentum of the wind away from the knots, rendering the large observed Doppler shifts of the knots unexplained. In any case, no such shocked tails are seen. Finally, the outflow must somehow reach the knots through the dense subsonic shell. No sign of a shell-outflow interface is observable except, perhaps, in NGC 6826 (see below). Table 2 summarizes the successes and failures of the two paradigms considered here.

So far the discussion has been general. However, individual microstructures may provide badly needed clues to the appropriate physical mechanisms. In NGC 6826, small triangular patches (morphologically similar to the outline of the ensemble of FLIERs) of bright [O III] and Hα emission appear between the tips of the interior hot bubble and the ensemble of FLIERs. Kinematic studies of the triangles (BPI) suggest that gas is being accelerated to the supersonic velocity of the FLIERs. In NGC 3242, gas is being similarly accelerated along loops of emission that connect the FLIERs to the hot bubble. Frank et al. (1996) argued that this is expected if the FLIERs are formed by gas sliding along the walls or a prolate cavity and converging at the tips of the loops. However, this process is viable only at wind velocities ≤ 150 km s^{-1}, whereas the wind velocity of the nucleus of NGC 3242 is presently 2200 km s^{-1} (Table 1).

Of special interest are the ansae of NGC 7009, whose relationship to the core is relatively easy to ascertain since the ansae are seen in isolation outside the nebula. We find smooth streamlike "jets" that connect each ansa to the tips of the hot bubble in the nebula. If these jets are outflowing material from the tips of the prolate bubble, then the ansae are being shaped, if not even accelerated, by winds. The small flare in the jets argues that their mechanical energy exceeds their thermal energy. Hence, if the sound (transverse) speed is 10 km s^{-1}, characteristic of emission-line gas at 10^4 K, then the flow speed of the jets is at least 30 km s^{-1}. Thus the jets and ansae are almost certainly true FLIERs lying near the plane of the sky. This interpretation is corroborated by the bow shocks with the ansae at their heads in a deep image of the ansae in NGC 7009 (Fig. 4). Ironically, the declining ionization state of the gas with radius is exactly the reverse of expectations, in which the highest shock velocities, temperatures, and ionization states of bow shocks are reached in their heads!

NGC 7662 contains microstructures with various classes of morphologies. Their geometry and kinematics qualify two of these classes, the serpentine and the head-tail microstructures, as FLIERs. The head-tail microstructures have most of the same properties as the FLIERs in NGC 3242 and NGC 6826, including their projected locations on the nebular symmetry axis. However, we cannot discern a kine-

TABLE 2

EXPLANATIONS FOR FLIERS IN TWO PARADIGMS

Observation	Fast, Dense (or Ram Pressure–confined) Bullets	Ambient Knots Immersed in Winds
Morphology/geometry:		
Small sizes ($\approx 10^{15}$ cm)	Intrinsic	Intrinsic
High surface brightness	Ionization front has high emission measure	Ionization front has high emission measure
Equal and opposite distances from star along nebular symmetry axis	Pairs of bullets ejected by star along spin axis? Formed by flows converging to symmetry axis??	??
Tails point outward	??	?? Perhaps winds accelerate ablated material; however, the process is inefficient for supersonic winds
Link to inner bubble (e.g., jets, flares, loops)	?? Perhaps the "refuse" of converging flows	These are evidence for winds through nebula
Location near nebular perimeter	??	??
Ionization:		
Low ionization relative to nebula	Bullets form as neutral gas? High density enhances recombination rate?	Knots form before stellar ionization starts; still being ionized
Ionization gradient with radius	Ionization front if interior is neutral	Ionization front if interior is neutral
Kinematics:		
High Doppler shifts	Intrinsic	?? Acceleration of neutral knots is inefficient
Equal but opposite Doppler shifts	Intrinsic	?? Must be result of knot formation process
Possible increasing Doppler shift from rim to FLIER	?? Possible Oort-Spitzer rocket effect	??
Conflicting cases	NGC 3242, 6826, 7662 (head-tail FLIERs only)	Ansae of NGC 7009
Most promising examples	Ansae of NGC 7009	NGC 3242, 6826

NOTE.—" ?" indicates a weak explanation; " ??" means highly problematic or no plausible explanation.

matic connection between these FLIERs and the hot bubble in NGC 7662. Serpentine FLIERs have the largest sizes and Doppler shifts of any of the microstructures. Speculatively, the serpentine FLIERs may be Oort-Spitzer rockets. Mellema et al. (1998) showed that shocks will be driven into the knots by the advance of the IF, producing a "squirt" of high-speed gas at high velocity in the forward direction just as the knots dissipate. The serpentine FLIERs have the characteristics of the jets so produced. The knots are broken up quickly once the low-ionization gas is ejected into the snake's tail. That may help to understand why the serpentine FLIERs at 11 and 1 o'clock are headless.

However, none of the conclusions based on anecdotal examples extrapolate successfully to the class of FLIERs as a whole. Perhaps FLIERs are highly individualistic in their formation or evolution.

More likely, the search for an entirely new paradigm is the most productive strategy for explaining FLIERs. Indeed, we are yet to identify even one conceptual model that does not conflict with the existing set of observations. New data are needed, if for no other reason, to help to stimulate new ideas—a process sometimes called "a fishing expedition" when a request for telescope time is denied!

Finally, it is important to note that low-ionization knots can also be found in some bipolar PNs at speeds of many hundreds of km s^{-1}, such as IRAS 17423−1755 (Riera et al. 1995) and MyCn 18 (Bryce et al. 1997). As yet, these have received little detailed study using *HST*. This is certainly a lucrative direction for future research.

It is a pleasure to thank Mr. Christian Ready for his enthusiastic and very capable help in preparing for the observations. We are grateful for the unpublished images supplied by George Jacoby and Howard Bond. Software developed by Mr. Eric Deutsch was immensely valuable. We have benefited from in-depth scientific discussions and ideas with Adam Frank, J. Patrick Harrington, Vincent Icke, and Garrelt Mellema, whose support has always been generous. This work was supported by NASA/STScI grant GO-6117. The *Hubble Space Telescope* is operated by the Space Telescope Science Institute under contract to NASA.

REFERENCES

Acker, A., Ochsenbein, F., Stenholm, B., Tylenda, R., Marcout, J., & Schohn, C. 1992, Strasbourg-ESO Catalogue of Galactic Planetary Nebulae (Garching: ESO)
Alexander, J., & Balick, B. 1997, AJ, 114, 713
Aller, L. H. 1941, ApJ, 93, 236
———. 1976, Mem. Soc. R. Sci. Liège, 9, 271
Balick, B. 1987, AJ, 94, 671
Balick, B., Gonzalez, G., Frank, A., & Jacoby, G. 1992, ApJ, 392, 582
Balick, B., Perinotto, M., Maccioni, A., Terzian, Y., & Hajian, A. 1994, ApJ, 424, 800 (Paper II)
Balick, B., Preston, H. L., & Icke, V. 1987, AJ, 94, 1641 (BPI)
Balick, B., Rugers, M., Terzian, Y., & Chengalur, J. N. 1993, ApJ, 411, 778 (Paper I)
Blöcker, T. 1995, A&A, 299, 755
Böhm, K.-H., & Goodson, A. P. 1997, in IAU Symp. 182, Herbig-Haro Flows and the Birth of Stars, ed. B. Reipurth & C. Bertout (Dordrecht: Kluwer), 47
Bohigas, J., López, J. A., & Aguilar, L. 1994, A&A, 291, 595
Breitschwerdt, D., & Kahn, F. D. 1990, MNRAS, 244, 521
Bryce, M., López, J. A., Holloway, A. J., & Meaburn, J. 1997, ApJ, 487, L161
Cerruti-Sola, M., & Perinotto, M. 1989, ApJ, 345, 339
Chevalier, R. A., & Luo, D. 1994, ApJ, 421, 225
Cliffe, J. A., Frank, A., Livio, M., & Jones, T. W. 1995, ApJ, 447, L49
Dopita, M. A. 1997, ApJ, 485, L41
Dwarkadas, V. V., & Balick, B. 1998, ApJ, 497, 267
Dyson, J. E., Hartquist, T. W., & Biro, S. 1993, MNRAS, 261, 430
Frank, A., Balick, B., & Livio, M. 1996, ApJ, 471, L53
Hajian, A. R., Balick, B., Terzian, Y., & Perinotto, M. 1997, ApJ, 487, 304 (Paper III)
Hamann, W.-R., Kudritzki, R.-P., Méndez, R. H., & Pottasch, S. R. 1984, A&A, 139, 459
Harrington, J. P., & Borkowski, K. J. 1994, BAAS, 26, 1469
Harrington, J. P., Seaton, M. J., Adams, S., & Lutz, J. H. 1982, MNRAS, 199, 517
Heap, S. R. 1986, in New Insights in Astrophysics, ed. E. J. Rolfe (Paris: ESA), 291
Henney, W. J., Raga, A. C., Lizano, S., & Curiel, S. 1996, ApJ, 465, 216
Holtzman, J. A., et al. 1995, PASP, 107, 156
Icke, V., Balick, B., & Frank, A. 1992, A&A, 253, 224
Kahn, F. D., & Breitschwerdt, D. 1990, MNRAS, 242, 505
Kahn, F. D., & West, K. A. 1985, MNRAS, 212, 837
Kwok, S., Purton, C. R., & FitzGerald, P. M. 1978, ApJ, 219, L125
Lame, N. J., & Pogge, R. W. 1996, AJ, 111, 2320
Lizano, S., Cantó, J., Garay, G., & Hollenbach, D. 1996, ApJ, 468, 739
Lopez, J. A., Meaburn, J., & Palmer, J. W. 1993, ApJ, 415, L135
López, J. A. Roth, M., & Tapia, M. 1993, A&A, 267, 194
López, J. A., Steffen, W., & Meaburn, J. 1997, ApJ, 485, 697
Meaburn, J., Clayton, C. A., Bryce, M., Walsh, J. R., Holloway, A. J., & Steffen, W. 1998, MNRAS, 294, 201
Mellema, G. 1995, MNRAS, 277, 173
Mellema, G., & Frank, A. 1995, MNRAS, 273, 401
Mellema, G., Raga, A. C., Cantó, J., Lundqvist, P., Balick, B., Steffen, W., & Noriega-Crespo, A. 1998, A&A, 331, 335
Méndez, R. H. 1991, in IAU Symp. 145, Evolution of Stars: The Photospheric Abundance Connection, ed. G. Michaud & A. V. Tutukov (Dordrecht: Kluwer), 375
Miranda, L. F., & Solf, J. 1992, A&A, 260, 397
O'Dell, C. R., & Handron, K. D. 1996, AJ, 111, 1630
Oort, J. H., & Spitzer, L., Jr. 1955, ApJ, 121, 6
Pauldrach, A., Puls, J., Kudritzki, R. P., Méndez, R. H., & Heap, S. R. 1988, A&A, 207, 123
Perinotto, M., Cerruti-Sola, M., & Lamers, H. J. G. L. M. 1989, ApJ, 337, 382
Reay, N. K., & Atherton, P. D. 1985, MNRAS, 215, 233
Riera, A., García-Lario, P., Manchado, A., Pottasch, S. R., & Raga, A. C. 1995, A&A, 302, 137
Schwarz, H. E., Corradi, R. L. M., & Melnick, J. 1992, A&AS, 96, 23
Terzian, Y. 1998, in IAU Symp. 180, Planetary Nebulae, ed. H. J. Habing & H. J. G. L. M. Lamers (Dordrecht: Kluwer), 29